The magnetic after-effect in amorphous and nanocrystalline Fe - Cu - Nb - Si - B alloys



1997 J. Phys.: Condens. Matter 9 4303

(http://iopscience.iop.org/0953-8984/9/20/025)

J. Phys.: Condens. Matter **9** (1997) 4303–4318. Printed in the UK PII: S0953-8984(97)76911-X

# The magnetic after-effect in amorphous and nanocrystalline Fe–Cu–Nb–Si–B alloys

J Zbroszczyk and W Ciurzyńska

Institute of Physics, Technical University of Częstochowa, Częstochowa, Poland

Received 5 August 1996, in final form 10 January 1997

**Abstract.** The magnetic relaxation phenomenon for the $Fe_{73.5}Cu_1Nb_3Si_{13.5}B_9$ alloy in the as-quenched state and after annealing is investigated. It is stated that the disaccommodation intensity distinctly decreases after the heat treatment of the sample at 673 K for 1 h due to the annealing out of some free volumes. Moreover, the intensity of the disaccommodation drops almost to zero after the sample crystallization occurs. From the results obtained, it becomes evident that the amorphous phase is the main source of the magnetic after-effect in the nanocrystalline samples. The present results are discussed under the assumption that the relaxation processes are described by a gaussian distribution in $\ln \tau$.

## 1. Introduction

Nanocrystalline alloys not only have potential technological applications, mainly due to their soft magnetic properties, but also they are interesting materials as regards fundamental research. These alloys, obtained usually by the appropriate annealing of amorphous ribbons, consist of $\alpha$-FeSi fine grains and some residual amorphous phase. The average grain size of the crystalline phase is about 10 nm [1, 2]. This fine grain structure leads to the excellent soft magnetic properties of the nanocrystalline alloys because of the diminished effective anisotropy due to the random anisotropy effect [2–7]. The microstructure of the nanocrystalline alloys can be studied by means of x-ray diffractometry, high-resolution transmission electron microscopy, or Mössbauer spectroscopy [8–11]. However, magnetic after-effects are structure sensitive [12, 13], and may also be used to detect local changes in the structure of these materials.

The basic cause of the magnetic after-effects occurring in materials is the presence of lattice imperfections. In crystalline materials, it is well known [14–16] that magnetic after-effects result from rearrangements of anisotropic atomic defects within domain walls in such a way as to lower the overall energy of a ferromagnet. The rearrangements of these defects are usually controlled by an activation energy, so there is a delay between the application of the magnetic field and the final equilibrium rearrangement of the various imperfections. For example, the so-called Richter after-effect [17] is caused by the hopping of C atoms between neighbouring octahedral interstitial sites in bcc $\alpha$-Fe. In amorphous alloys, empty spaces exist between the ions, also called free volumes, and these act as vacancy-like defects which enable the reorientation of atom pairs to occur [13, 18]. This reorientation, in general, takes place via thermally activated processes, and is therefore strongly temperature dependent.

The magnetic properties of the amorphous alloys produced by a rapid-quenching method are metastable over long periods of time [19], and the magnetic relaxation

0953-8984/97/204303+16$19.50  

processes occurring in these materials are of both scientific and practical interest. In nanocrystalline materials, two different magnetic phases (the $\alpha$-FeSi phase and the amorphous matrix) coexist, and investigation of the magnetic after-effect can additionally enable one to determine the phase contribution to this effect [20]. The magnetic after-effect in the amorphous and nanocrystalline Fe–Cu–Nb–Si–B alloys has scarcely been investigated [21–23].

In the present paper we study the disaccommodation of the initial magnetic susceptibility (which is one of the magnetic after-effect phenomena) and microstructure of the amorphous and nanocrystalline $Fe_{73.5}Cu_1Nb_3Si_{13.5}B_9$ alloys.

## 2. Experimental details

### *2.1. Samples and magnetic measurements*

Amorphous ribbons of the $Fe_{73.5}Cu_1Nb_3Si_{13.5}B_9$ alloy were prepared by the rapid-quenching technique on a single roller. The width and thickness of the ribbons were 10 mm and 15 $\mu$m, respectively. Using a completely automatic set-up, the initial magnetic susceptibility $\chi(t, T)$ was measured.

The magnetic after-effect was observed as a disaccommodation, i.e. a decrease over time of the initial susceptibility $\chi(t, T)$, following the demagnetization of the samples. The experimental results are presented as isochronal curves:

$$\Delta(1/\chi) = 1/\chi_2 - 1/\chi_1 = f(T) \tag{1}$$

where $1/\chi_1$ and $1/\chi_2$ are reciprocal magnetic susceptibilities at the times $t_1 = 2$ s and $t_2 = 120$ s after demagnetization, respectively. Before each measurement the samples were demagnetized by applying a sinusoidal magnetic field of frequency equal to 120 Hz with an amplitude decreasing exponentially from 500 A m$^{-1}$ to zero over 1.1 s. These investigations were carried out for toroidal samples of 30 mm inner diameter by applying an ac magnetizing field of frequency $f = 2$ kHz and amplitude $H = 0.16$ A m$^{-1}$. Additionally, for the same sample the $\Delta(1/\chi) = f(H)$ dependence in the magnetizing field range from 0.03 to 2.4 A m$^{-1}$ was studied.

The investigations were carried out for samples in the as-quenched state, after pre-annealing at 673 K for 1 h and after subsequent annealing at 823 K for 10 and 60 min (cumulative annealing) in a vacuum of 0.01 Pa.

### *2.2. Investigations of the sample microstructure*

The microstructure of the samples was examined using Mössbauer spectroscopy and x-ray diffractometry. In this paper, the Mössbauer effect is used to obtain information concerning the magnetization distribution, the average hyperfine field at the $^{57}$Fe nuclei, and the phase composition of the samples. Additionally, the degree of order in the crystalline phase was determined. The average hyperfine field was obtained from the hyperfine-field distributions which were evaluated according to the Hesse–Rübartsch method [24]. Information about the magnetization distribution in the samples can be obtained from the analysis of the line intensities in the Zeeman sextets. As this problem is rather complicated in the case of broad and strongly overlapping lines, we recorded Mössbauer spectra of the as-quenched sample in three configurations (A, B, and C; see figure 1) according to the magic-angle method [25, 26]. From the analysis of these spectra, the spin populations $P_x$, $P_y$, and $P_z$ along the

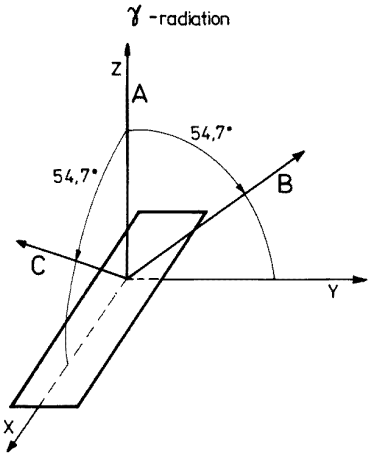


**Figure 1.** Configurations of the sample, and orientations of the $\gamma$-radiation.

principal axis of minimum texture were determined according to the equations

$$P_z = \langle \cos^2 \varphi \rangle_A \tag{2}$$

$$P_y - P_x = \tfrac{2}{3}(\langle \cos^2 \varphi \rangle_B - \langle \cos^2 \varphi \rangle_C) \tag{3}$$

and

$$\langle \cos^2 \varphi \rangle_B + \langle \cos^2 \varphi \rangle_C = \tfrac{2}{3} \tag{4}$$

where $\varphi$ (the angle between the directions of the radiation and the magnetic moment) is given by

$$\frac{4(1 - \langle \cos^2 \varphi \rangle)}{3 + 3\langle \cos^2 \varphi \rangle} = \frac{A_{2,5}}{A_{1,6}}. \tag{5}$$

Here, $A_{2,5}/A_{1,6}$ are the ratios of the second and first line intensities in the Zeeman sextets. The Mössbauer spectra were analysed with a least-squares method by superimposing sets of Zeeman sextets. In the fitting procedure, various authors used four [27–30], five [31, 32], six [11], or seven sextets [33] corresponding to the crystalline phase of the nanocrystalline $Fe_{73.5}Cu_1Nb_3Si_{13.5}B_9$ alloy. As well as the $\alpha$-FeSi phase of $DO_3$ structure, iron–boron phases were also found [33]. However, the amorphous matrix was interpreted in terms of one sextuplet of broadened lines [11, 27], one broad-line sextet [32], two sextets [29, 31], or one sextet and one doublet [30].

We obtained the best fit by decomposing the Mössbauer spectra of the nanocrystalline samples into seven components: five sextets for the $\alpha$-FeSi phase associated with iron atoms having eight, seven, six, five, and four Fe atoms as the nearest neighbours, and two broadened sextets corresponding to the residual amorphous phase (similarly to the results of [31]). The linewidths in the Zeeman sextets corresponding to the crystalline phase were kept constant, and equal to 0.50 and 0.46 mm $s^{-1}$ for the samples annealed at 823 K for 10 and 60 min, respectively. However, the linewidths corresponding to the amorphous matrix were fitted. We assumed that the amorphous matrix consists of low- and high-field components. The low-field component may correspond to the regions, near the crystalline grains, which contain more non-ferromagnetic atoms such as B, Cu, and Nb [31]. However, the microstructure of the high-field component is similar to that of the amorphous alloy after annealing at 673 K for 1 h. No Fe borides, such as are reported in [33], have been found in our samples.

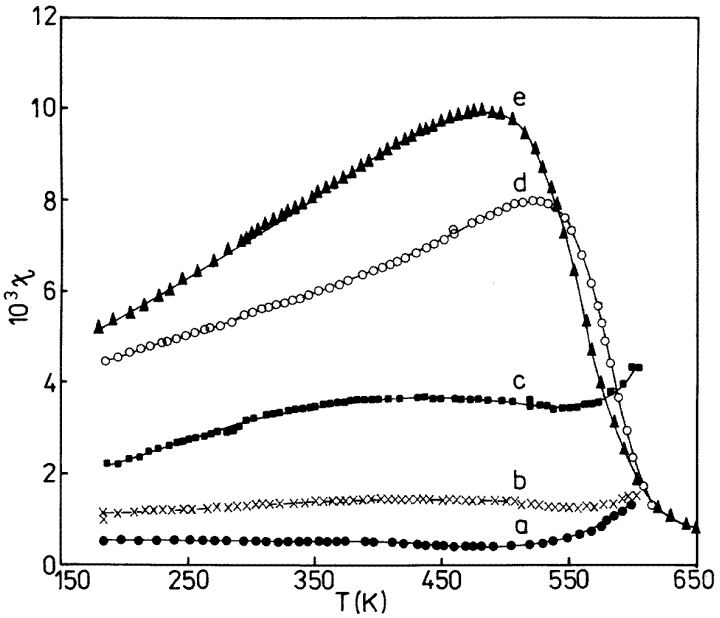


**Figure 2.** The temperature dependence of the initial susceptibility for the $Fe_{73.5}Cu_1Nb_3Si_{13.5}B_9$ alloy: as-quenched (first run) (a), second run (b), annealed at 673 K for 1 h (c), and annealed at 823 K for 10 min (d) and for 1 h (e).

In order to determine the volume fraction of the amorphous matrix $V_{am}$ and its iron content $Fe_{am}$, we assume that during the crystallization of the samples pre-annealed at 673 K for 1 h no significant structural changes occur in the amorphous matrix. However, a decrease of the iron content (by about 10 at.%) takes place, and the assumption that the average hyperfine field is proportional to the iron content in the amorphous phase [34, 35] is a good approximation in this case. Hence, the iron content in the amorphous matrix, and its volume fraction were calculated from the equations

$$\mathrm{Fe}_{am} = \frac{73.5 \text{ at.\%} \langle H_{am} \rangle}{\langle H_{am,673} \rangle} \tag{6}$$

and

$$V_{am} = \frac{R \langle H_{am,673} \rangle}{\langle H_{am} \rangle} \tag{7}$$

where $R$ is the relative area of subspectra corresponding to the amorphous matrix obtained from analysis of the Mössbauer spectra, and $\langle H_{am,673} \rangle$ and $\langle H_{am} \rangle$ are the average hyperfine fields obtained for the amorphous sample annealed at 673 K for 1 h and the amorphous matrix, respectively.

Knowing the volume fraction of the amorphous matrix and its iron content, we can calculate the volume fraction of the crystalline phase and its composition. In these calculations we assumed the same probability of recoil-free absorption (the Debye–Waller factor $f = 0.77$) for the amorphous matrix and the crystalline $\alpha$-FeSi phase. The value of the Debye–Waller factor was obtained for the Debye temperature $\theta_D = 400$ K. This seems to be justified because the Debye temperatures $\theta_D$ obtained from Mössbauer investigations for the amorphous $Fe_{69}Si_{21}B_{10}$ alloy [36] and metallic iron [37] are equal to $400 \pm 20$ K and $400 \pm 30$ K, respectively.

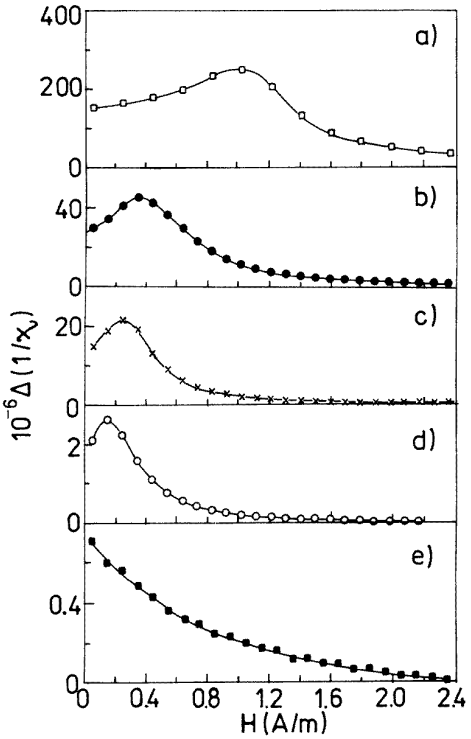


**Figure 3.** The field dependence of the magnetic after-effect for the samples: in the as-quenched state (a), after the second run (b), annealed at 673 K for 1 h (c), and annealed at 823 K for 10 min (d) and for 1 h (e).

The short-range-order parameter $\alpha_s$ of the crystalline $\alpha$-FeSi phase was calculated using the formula for binary Fe–Si alloys [38]:

$$\alpha_s = \frac{n - n_0}{n_0} \tag{8}$$

where $n_0$ is the average number of Si atoms in the neighbourhood of Fe atoms arranged randomly in a bcc lattice, obtained from a binomial distribution, and $n$ is the number of these atoms in the alloy investigated:

$$n_0 = c_{\mathrm{Si}} l_{nn} \tag{9}$$

where $c_{\mathrm{Si}}$ is the silicon concentration, $l_{nn}$ (equal to 8) is the number of nearest neighbours in a bcc lattice, and

$$n = l_{nn} - \sum_{i=4}^{8} p_i i \tag{10}$$

where $p_i = R_i / \sum_{i=4}^{8} R_i$ and $R_i$ are the relative areas of the sextets corresponding to the iron atoms having eight, seven, six, five, and four iron atoms as the nearest neighbours.

The studies of the microstructure were performed for the samples after the same treatments as were used for the magnetic measurements.

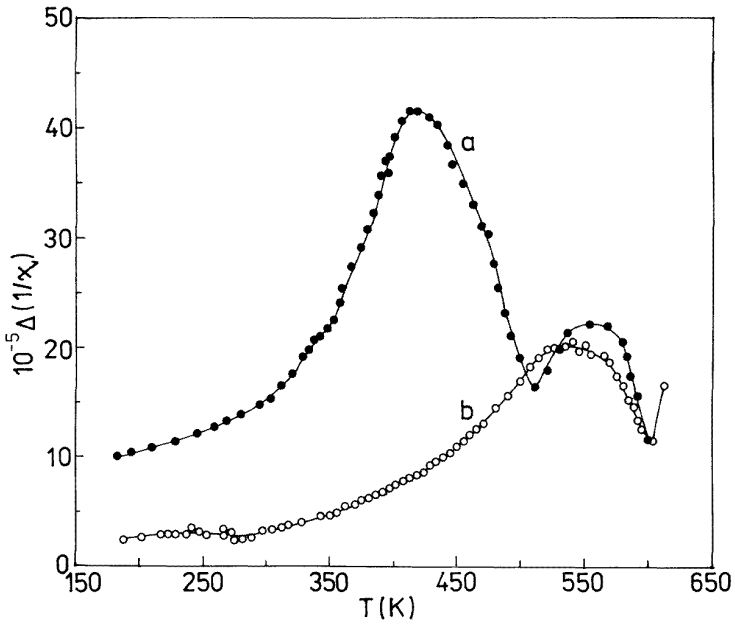


**Figure 4.** After-effect spectra for the $Fe_{73.5}Cu_1Nb_3Si_{13.5}B_9$ alloy: in the as-quenched state (first run) (a), and the second run (b).

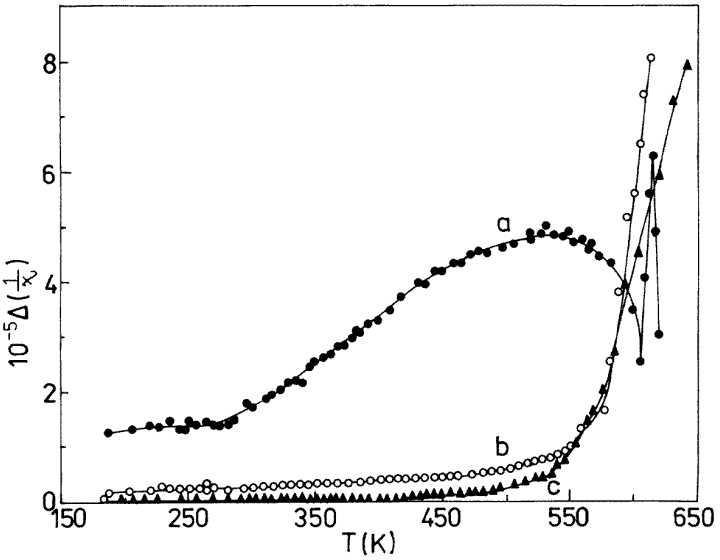


**Figure 5.** After-effect spectra for the $Fe_{73.5}Cu_1Nb_3Si_{13.5}B_9$ alloy: annealed at 673 K for 1 h (a), and annealed at 823 K for 10 min (b) and for 1 h (c).

## 3. Results

The temperature dependence of the initial susceptibility measured 2 s after demagnetization for the as-quenched and annealed samples is presented in figure 2. It is seen that the initial

susceptibility distinctly increases with annealing temperature and time.

Figure 3 shows the disaccommodation measured at $T = 290$ K versus the magnetizing field amplitude for the $Fe_{73.5}Cu_1Nb_3Si_{13.5}B_9$ alloy in the as-quenched state, after the second run, and after subsequent annealing at 673 K for 1 h, and at 823 K for 10 min and for 1 h. As can be seen from this figure, the disaccommodation distinctly decreases after the cumulative annealing of the sample, and the maxima of the $\Delta(1/\chi) = f(H)$ curves shift towards lower magnetizing fields. The stabilization field $H_s$ (the magnetizing field at which $\Delta(1/\chi)$ reaches a maximum value) determined from those curves is presented in table 1. In this table, the coercivity for the as-quenched and annealed samples is also shown.

**Table 1.** The average hyperfine field at $^{57}$Fe nuclei ($B_{eff}$), the second line intensity in the Zeeman sextets ($\langle A_{2,5}\rangle$), the volume fraction of the amorphous phase ($V_{am}$), the iron contents in the amorphous and crystalline phases ($Fe_{am}$, $Fe_{cr}$), the short-range-order parameter ($\alpha_s$), the coercivity ($H_c$), and the stabilization field ($H_s$) for the as-quenched and annealed $Fe_{73.5}Cu_1Nb_3Si_{13.5}B_9$ samples.

| Sample | $B_{eff}$ (T) | $A_{2,5}$ | $V_{am}$ | $Fe_{am}$ | $Fe_{cr}$ | $\alpha_s$ | $H_c$ (A m$^{-1}$) | $H_s$ (A m$^{-1}$) |
|---|---|---|---|---|---|---|---|---|
| As-quenched | 20.7 | 2.3 | 1 | 73.5 | — | — | 11.0 | 1.05 |
| 673 K/1 h | 21.3 | 2.4 | 1 | 73.5 | — | — | 4.0 | 0.24 |
| 823 K/10 min | 23.6 | 3.7 | 0.54 | 71.1 | 76.3 | 0.21 | 2.0 | 0.14 |
| 823 K/1 h | 23.6 | 3.3 | 0.46 | 62.7 | 82.6 | 0.52 | 1.7 | $< 0.04$ |

The isochronal relaxation spectra of the $Fe_{73.5}Cu_1Nb_3Si_{13.5}B_9$ ribbon are shown in figures 4 and 5. It is seen (figure 4) that the disaccommodation $\Delta(1/\chi)$ for the as-received sample (first run) increases to a maximum at about 420 K; a further smaller maximum occurs at about 550 K. The curve $\Delta(1/\chi) = f(T)$ (figure 4) obtained for the same sample during the second run (repeated measurement) shows a very broad maximum at about 540 K. The results obtained during the second and third runs coincided very well, so these are not shown in figure 4. The disaccommodation intensity is reduced after annealing this sample at 673 K for 1 h (figure 5). After subsequent treatment of the sample at 823 K for 10 min and then 50 min it is seen that between 200 and 520 K no relaxation processes are observed, apart from an almost temperature-independent relaxation background; above 520 K, $\Delta(1/\chi)$ increases with temperature.

**Table 2.** The ratios of the line intensities $A_{2,5}/A_{1,6}$ in the Zeeman sextets, and the spin populations ($P_x$, $P_y$, $P_z$—according to figure 1, from equations (3)–(5)) (with $\langle\cos^2\theta\rangle_B + \langle\cos^2\theta\rangle_C = 0.67$) for amorphous $Fe_{73.5}Cu_1Nb_3Si_{13.5}B_9$ alloy.

| Sample | Configuration | $A_{2,5}/A_{1,6}$ | $P_x$ | $P_y$ | $P_z$ |
|---|---|---|---|---|---|
| As-quenched | A | 0.77 | | | 0.27 |
| As-quenched | B | 0.70 | | 0.37 | |
| As-quenched | C | 0.73 | 0.36 | | |
| Annealed at 673 K for 1 h | A | 0.80 | | | 0.25 |

In figure 6 Mössbauer spectra (recorded in the A configuration; see figure 1) for the as-quenched and annealed samples are presented. The Mössbauer spectra taken for the as-quenched samples and the samples annealed at 673 K for 1 h (figure 6, spectra (a) and (b)) each consist of six broadened lines, which is typical for amorphous materials. However, after

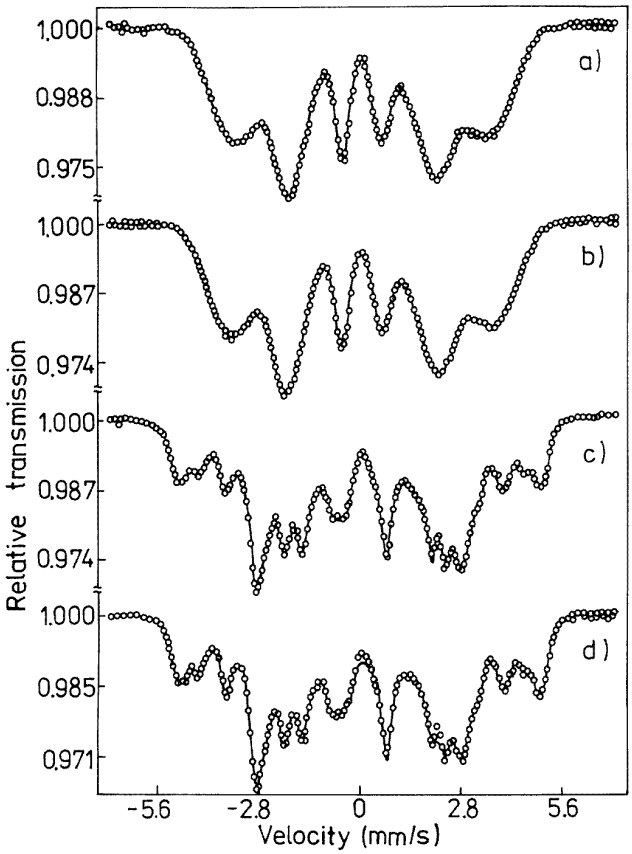


**Figure 6.** Mössbauer spectra for the $Fe_{73.5}Cu_1Nb_3Si_{13.5}B_9$ alloy in the as-quenched state (a), and after annealing at 673 K for 1 h (b), and at 823 K for 10 min (c) and for 1 h (d).

annealing the samples at 823 K, narrow lines corresponding to the crystalline phase appear (figure 6, spectra (c) and (d)). The results obtained from numerical analysis of these spectra are listed in table 1. Moreover, figure 7 shows the Mössbauer spectra (a) and corresponding hyperfine-field distributions (b) for the as-quenched sample in two configurations, B and C (see figure 1).

The ratios of line intensities $A_{2,5}/A_{1,6}$ in the Zeeman sextets, and the spin populations along the principal axis of the minimum texture are presented in table 2. The results for the samples in configuration A are obtained from the analysis of the Mössbauer spectra shown in figure 6.

## 4. Discussion

The samples investigated are fully amorphous in the as-quenched state and after annealing at 673 K for 1 h. This is confirmed by Mössbauer spectroscopy (figure 6, table 1) and x-ray diffractometry. After the heat treatment of the sample at 823 K, $\alpha$-FeSi grains appear (figure 6, table 1). Moreover, it is seen that the magnetization distribution depends on the annealing temperature (table 1); the second line intensities in the Zeeman sextets change

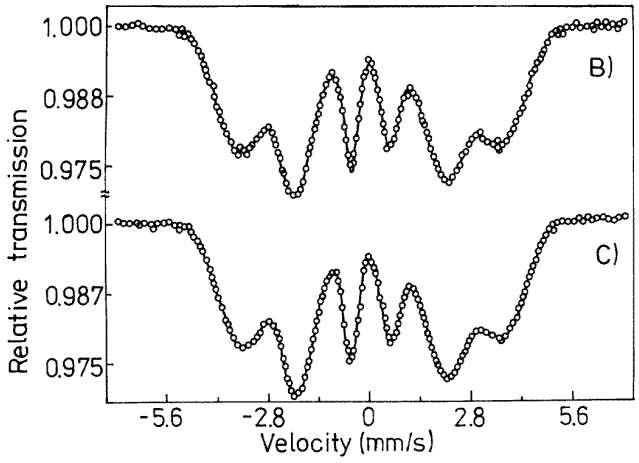


(a)

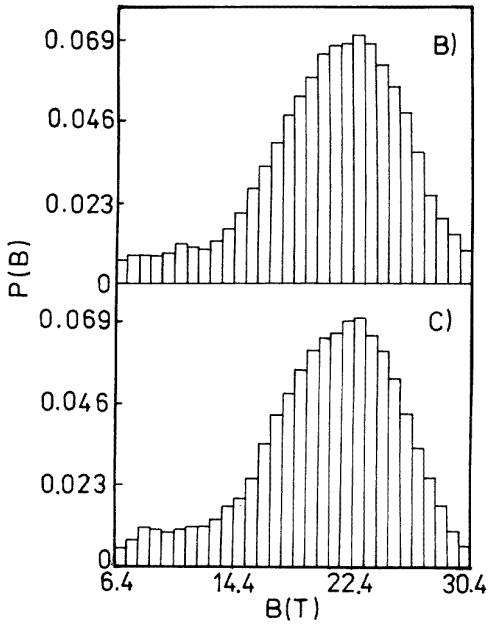


(b)

**Figure 7.** Mössbauer spectra (a) and the corresponding hyperfine-field distributions (b) for the as-quenched sample in configurations B and C (see figure 1).

from 2.3 in the as-quenched state to 3.7 after annealing the samples at 823 K for 10 min.

It is known that the magnetic moment distribution is determined by the demagnetizing interaction, which favours moment orientation in the ribbon plane, and by the local anisotropy, which turns the moments towards the local easy directions. Because of the first effect, the spin population in the $z$-axis direction ($P_z$) is a bit smaller than $P_y$ and $P_x$ (table 2). However, in the as-quenched ribbons there is a complex anisotropy distribution caused by complex internal stresses introduced during the preparation of the ribbons. Thus,

the magnetization vector is almost randomly distributed in the as-quenched sample; the ratios of the line intensities in the Zeeman sextets ($A_{1,6}$:$A_{2,5}$:$A_{3,4} = 3$:$\langle A_{2,5}\rangle$:1) are approximately equal to 3:2:1 (figure 1, tables 1 and 2). During the annealing of the sample at 673 K for 1 h the internal stresses are partially relieved, and the spin population in the $z$-axis direction (figure 1) decreases (table 2), so, the tendency for the magnetization vector to align parallel to the ribbon surface increases slightly (table 1). Moreover, enhancement of the average hyperfine field ($B_{eff}$) is observed (table 1), which indicates that the packing density increases due to the annealing out of some free volumes. The heat treatment of the samples at 823 K leads to further annealing of free volumes in the amorphous phase and stress relief of the samples, and the appearance of $\alpha$-FeSi grains. The diameter of the randomly distributed grains is smaller than the exchange length [2–7], and the magnetization cannot follow the randomly oriented easy axis of each individual grain because the magnetic moments are forced to align parallel within several grains. As a consequence of these effects, the magnetization vector aligns almost parallel to the ribbon surface (an increase of $A_{2,5}$; see table 1). However, after the cumulative annealing of the samples at 823 K for 1 h, slight decreases of the second line intensities in the Zeeman sextets are observed (table 1). This effect seems to indicate that the cumulative annealing influences the formation of the nanostructure in this sample. We can see (table 1) that the iron content in the crystalline phase depends on the annealing time. The $\alpha$-FeSi grains grow from the nuclei which are formed in the iron-rich regions due to the diffusion of Cu, Nb, and B atoms in these regions into the surrounding amorphous phase [39, 40]. When the annealing time is short, the diffusion of these atoms may be incomplete. With an increase of the annealing time, more and more of the Cu, Nb, and B atoms diffuse into the amorphous matrix, causing an increase of the iron content in the crystalline phase (table 1). Moreover, the iron content in the amorphous matrix is reduced (table 1). The presence of an amorphous matrix with reduced iron content is widely accepted. As for the crystalline $\alpha$-FeSi phase, some research has found that it has the $DO_3$ ordered structure [11, 27, 29, 30, 32, 33]. However, a few papers have reported a bcc iron–silicon phase [28, 31].

It is known that up to 10 at.% silicon content in the $\alpha$-FeSi phase, Si atoms will go into each atomic site with equal probability. If the silicon content is higher than 10 at.%, the ordered $DO_3$ structure will appear [41, 42]. In Fe–25 at.% Si alloy, 1/3 of Fe atoms have eight iron atoms as the nearest neighbours (nn), and 2/3 of Fe atoms have four Si nn atoms and four Fe nn atoms. If the Fe–Si alloy contains less than 25 at.% silicon, Fe atoms will randomly occupy some of the Si sites, which creates additional iron sites. From analysis of the Mössbauer spectra, we found that the ratios of the probabilities (equal to the ratios of the relative areas of the corresponding sextets) for iron atoms to have 8, 7, 6, 5, or 4 Fe atoms as the nearest neighbours in the crystalline $\alpha$-FeSi phase are equal to $8Fe_{nn}$:$7Fe_{nn}$:$6Fe_{nn}$:$5Fe_{nn}$:$4Fe_{nn} = 0.20$:0.16:0.08:0.28:0.27 and 0.20:0.19:0.18:0.16:0.27 for the samples annealed at 823 K for 10 min and 1 h, respectively. However, from the binomial distribution we obtained $8Fe_{nn}$:$7Fe_{nn}$:$6Fe_{nn}$:$5Fe_{nn}$:$4Fe_{nn} = 0.11$:0.29:0.31:0.19:0.07 and 0.23:0.36:0.27:0.11:0.03 for the samples annealed at 823 K for 10 and 60 min, respectively. It is seen that the probabilities of occurrence of 5 and 4 Fe atoms as nn are larger than those in the random model. Moreover, the results obtained from Mössbauer spectroscopy investigations are different from those for the $DO_3$ structure [38]. Thus, we may conclude that the atomic arrangement of Si atoms in the crystalline $\alpha$-FeSi phase is not random but has short-range order (table 1). Moreover, one can notice that the $\alpha$-FeSi phase becomes more ordered with the increase of the annealing time (table 1).

The microstructure of the samples influences their magnetic properties in the as-quenched state and after annealing. The as-received ribbons exhibit rather poor soft magnetic

properties: i.e., low initial magnetic susceptibility (figure 1) and high coercivity, stabilization field (table 1), and disaccommodation intensity (figures 3 and 4) due to the high density of structural defects (free volumes, agglomerations of free volumes) which give rise to elastic stresses in the amorphous alloys [43].

From the results obtained for magnetic disaccommodation of the as-quenched samples (figure 4), it is possible to conclude that during the first run the irreversible annealing processes appear to occur simultaneously with the reversible ones. The irreversible relaxations are connected with mobile atom pairs in the environment of these free volumes, which change their configuration. These atom pairs become immobile after the annealing of the excess free volumes [13, 18, 44] which leads to the vanishing of the relaxation at 420 K (figure 4). So, the relaxation spectrum obtained during the second run shows only a very broad maximum at 540 K, and this is caused by the reversible processes which may be considered as the reorientation of mobile atom pairs between two energetically equivalent configurations separated by a potential barrier [13, 18]. These processes occur due to the small displacement of free volumes which causes the reorientation of pair axes. After annealing the samples at 673 K for 1 h, a distinct increase of the initial susceptibility (figure 2) and decrease of the disaccommodation amplitude $\Delta(1/\chi)$, stabilization field, and coercivity are observed (figures 3 and 5, table 1). These changes are connected with the further annealing out of some free volumes [13, 18, 45] and the stress relief of the samples. These results are confirmed by Mössbauer spectroscopy investigations (table 1); the enhancement of the average hyperfine field ($B_{eff}$) indicates that the packing density increases after annealing the sample, and the increase of the second line intensity in Zeeman sextets shows that the magnetization vector exhibits a larger tendency to align parallel to the ribbon surface.

The isochronal disaccommodation curves obtained for the amorphous samples (during the second run and after annealing at 673 K for 1 h) show broad maxima at about 540 K. From the Arrhenius law for $T = T_p$ (the peak temperature) we obtain

$$T_p = \frac{E}{k \ln(\tau_p/\tau_0)} \tag{11a}$$

where $\tau_p$ is the relaxation time ($\tau$) at the peak temperature ($T_p$), $\tau_0$ is the pre-exponential factor, $k$ the Boltzmann constant, and $E$ the activation energy. $\tau_p$ is expressed as

$$\tau_p = \frac{t_2 - t_1}{\ln(t_2/t_1)} \tag{11b}$$

which is obtained from the maximum of the isochronal disaccommodation curve for a single Debye process, i.e.

$$\Delta(1/\chi) = I\{\exp[-(t_1/\tau)] - \exp[-(t_2/\tau)]\} \tag{12}$$

where $I$ is the disaccommodation intensity.

One can see from equations (11*a*) and (11*b*) that with the increase of $t_2$ the peak temperature shifts to lower temperatures. This behaviour proves the migrational origin of the observed relaxation spectra [15], and is observed for the isochronal disaccommodation curves of the amorphous samples. In figure 8 the relaxation spectra obtained during the second run for different measuring times $t_2$, as an example, are shown.

Generally, for an analysis of the disaccommodation curves for amorphous materials, the box distribution function of relaxation times $p(\tau)$ is usually assumed:

$$p(\tau) = \begin{cases} \dfrac{1}{\tau \ln(\tau_2/\tau_1)} & \text{for } \tau_1 < \tau < \tau_2 \\ 0 & \text{in all other cases.} \end{cases} \tag{13}$$

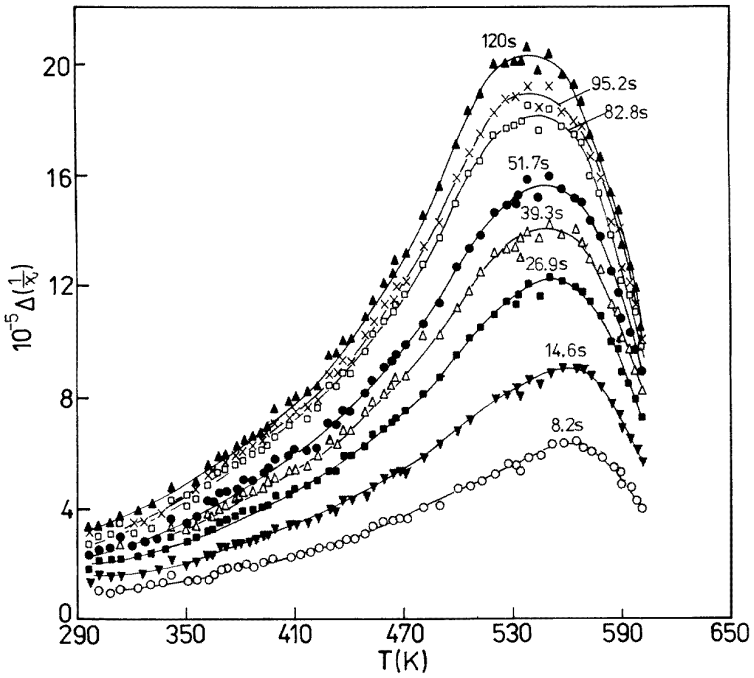


**Figure 8.** Isochronal relaxation spectra of the amorphous $Fe_{73.5}Cu_1Nb_3Si_{13.5}B_9$ alloy obtained during the second run for different measuring times $t_2$.

The distribution function $p(\tau)$ is approximated by a series of box distribution functions of $E$ between a lower activation energy $E_i$ and an upper limit $E_{i+1}$ [13, 18].

In our paper, we use a gaussian distribution in $\ln\tau$ [46], which is more likely to describe real processes in amorphous materials. In this case the distribution function is given by

$$p(\tau) = \frac{1}{\sqrt{\pi}\beta}\exp\left[-\left(\frac{\ln(\tau/\tau_m)}{\beta}\right)^2\right] \tag{14}$$

where $\tau_m$ is an average value of the relaxation time, and $\beta$ is a distribution parameter.

Furthermore, $\tau_m$ fulfils the Arrhenius law:

$$\tau_m = \tau_{0m}\exp(E_m/kT) \tag{15}$$

where $\tau_{0m}$ is a pre-exponential factor, and $E_m$ an average activation energy. The isochronal relaxation spectrum consisting of one process can be described by the integral

$$\Delta\left(\frac{1}{\chi}\right) = \int_{-\infty}^{+\infty}\frac{1}{\sqrt{\pi}\beta}I_p\frac{T_p}{T}\left\{\exp\left[-\left(\frac{t_1}{\tau}\right)\right]-\exp\left[-\left(\frac{t_2}{\tau}\right)\right]\right\} \times \exp\left[-\left(\frac{\ln(\tau/\tau_m)}{\beta}\right)^2\right]\mathrm{d}\ln\tau \tag{16}$$

where $I_pT_p/T = I$ denotes the disaccommodation intensity; $I_p$ is the disaccommodation intensity at the peak temperature ($T_p$). After introducing a variable $z = \ln(\tau/\tau_m)$, and under the assumption that the relaxation spectrum can be described as a superposition of

the individual processes, we obtain

$$\Delta\left(\frac{1}{\chi}\right) = \sum_{i=1}^{n} \frac{1}{\sqrt{\pi}\beta_i} \int_{-3\beta_i}^{+3\beta_i} I_{p_i} \frac{T_{p_i}}{T} \left\{ \exp\left[-\left(\frac{t_1}{\tau_{mi} e^z}\right)\right] - \exp\left[-\left(\frac{t_2}{\tau_{mi} e^z}\right)\right]\right\} \times \exp\left[-\left(\frac{z}{\beta_i}\right)^2\right] dz. \tag{17}$$

The average relaxation time $\tau_{mi}$ is given by

$$\tau_{mi} = \tau_p \exp\left[\frac{E_{mi}}{k}\left(\frac{1}{T} - \frac{1}{T_{pi}}\right)\right] \tag{18}$$

where $\tau_p$ is given by equation (11*b*) for $t_1 = 2$ s and $t_2 = 120$ s after demagnetization of the sample.

We assume limiting values for $z$ of $\pm 3\beta$, which approximately correspond to $\pm\infty$. From a numerical analysis of the relaxation spectra, the following parameters for individual processes are determined: the disaccommodation intensity $I_{pi}$ at $T_{pi}$ (the peak temperature), the average activation energy $E_{mi}$, and the distribution parameter $\beta_i$. Furthermore, the pre-exponential factor $\tau_{0mi}$ is given by

$$\tau_{0mi} = \tau_p \exp(-E_{mi}/kT_{pi}). \tag{19}$$

Under the assumption that the gaussian distribution in $\ln\tau$ corresponds to the distribution of the activation energies $E_i$, we obtain

$$E_{mi} - \beta_i kT_{pi} \leqslant E_i \leqslant E_{mi} + \beta_i kT_{pi}. \tag{20}$$

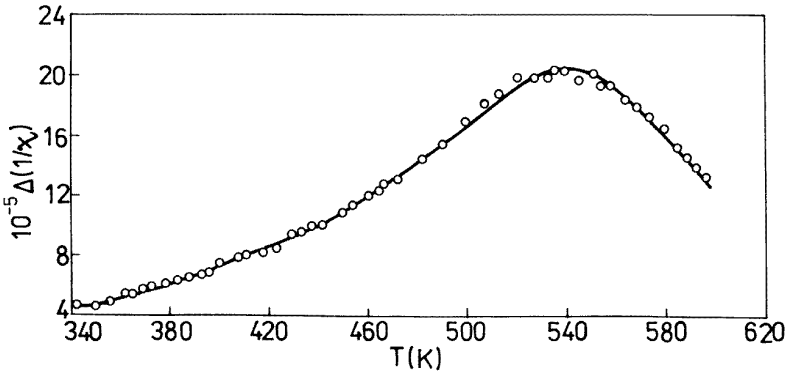


**Figure 9.** The fitted isochronal $\Delta(1/\chi) = f(T)$ curve and experimental points obtained for the amorphous $Fe_{73.5}Cu_1Nb_3Si_{13.5}B_9$ alloy during the second run.

We decomposed the relaxation spectra $\Delta(1/\chi) = f(T)$ obtained during the second run and after annealing the same sample at 673 K for 1 h using the gaussian distribution in $\ln\tau$. The results obtained from this analysis are listed in table 3. The relaxation background is assumed to have a linear temperature dependence. The fitted curves and experimental points are shown in figures 9 and 10. It is seen (figures 9 and 10) that a good fitting is obtained after decomposition of the experimental relaxation spectra into three elementary processes.

It is worth noticing that the intensity of the disaccommodation in the temperature range from 200 to 520 K for the nanocrystalline sample (after annealing at 823 K) is much lower

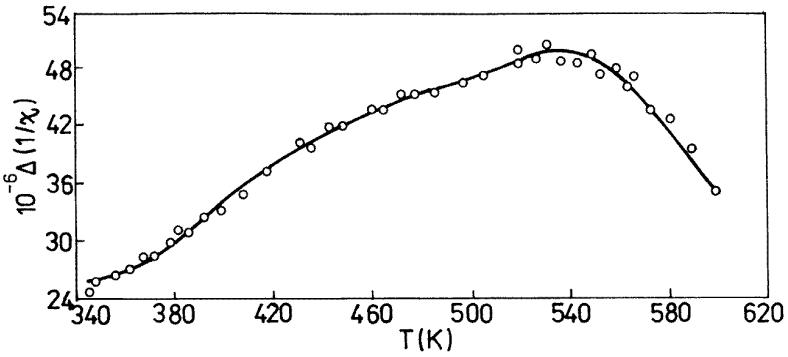


**Figure 10.** Experimental points and the fitted relaxation spectrum for the $Fe_{73.5}Cu_1Nb_3Si_{13.5}B_9$ sample annealed at 673 K for 1 h.

**Table 3.** The peak temperature ($T_p$), the intensity of the process ($I_p$) at $T_p$, the average activation energy ($E_m$), the pre-exponential factor ($\tau_{0m}$), and the activation energy ($E$) (from equation (20)) obtained for the $Fe_{73.5}Cu_1Nb_3Si_{13.5}B_9$ alloy.

| Sample | Process | $T_p$ (K) | $10^{-6}I_p$ | $E_m$ (eV) | $10^{-15}\tau_0$ (s) | $E$ (eV) |
|---|---|---|---|---|---|---|
| Second | I | 428 | 46 | 1.33 | 5.8 | $1.18 \leqslant E \leqslant 1.48$ |
| run | II | 493 | 89 | 1.53 | 6.9 | $1.42 \leqslant E \leqslant 1.64$ |
| | III | 547 | 122 | 1.69 | 7.6 | $1.60 \leqslant E \leqslant 1.78$ |
| Annealed, | I | 432 | 22 | 1.35 | 5.4 | $1.20 \leqslant E \leqslant 1.50$ |
| 673 K/1 h | II | 498 | 23 | 1.59 | 2.6 | $1.44 \leqslant E \leqslant 1.74$ |
| | III | 553 | 20 | 1.73 | 4.7 | $1.64 \leqslant E \leqslant 1.82$ |

than that for the amorphous samples (figures 4 and 5). In spite of the increase of the crystalline volume fraction up to 54% (table 1), the contribution of the $\alpha$-FeSi phase to the magnetic after-effect is not evident (figure 5).

From the results obtained, one may conclude that the magnetic disaccommodation in the nanocrystalline alloys is caused by the relaxation processes occurring in the amorphous matrix. The low disaccommodation intensity for the nanocrystalline samples is connected with the annealing out of most of the free volumes in the amorphous matrix during the heat treatment of the sample at 823 K. The distinct increase of the disaccommodation intensity in the amorphous samples (figures 4 and 5) above 600 K seems to be connected with the rapid change of the material constants near the Curie temperature of the amorphous matrix (the Hopkinson maximum) [13, 18, 47]. A similar effect occurs during measurements of the magnetic susceptibility, which shows a sharp peak in a narrow temperature region around the Curie temperature. This behaviour of the magnetic susceptibility was observed for both the amorphous [48] and the crystalline [21, 49, 50] materials.

As for the increase of the disaccommodation intensity for nanocrystalline samples near the Curie temperature of the amorphous matrix (figure 5), the phenomenon is more complicated than for the amorphous alloys. According to the random-anisotropy model, the average anisotropy constant $\langle K_1 \rangle$ for an assembly of randomly oriented grains can be expressed [2–6] as

$$\langle K_1 \rangle = K_1^4 D^6 / A^3 \tag{21}$$

where $K_1$ is the magnetocrystalline anisotropy constant, $D$ is the grain diameter, and $A$ is the exchange energy constant. Since the exchange energy constant $A$ varies as $[M_{s,am}(T)]^2$, (where $M_{s,am}(T)$ is the saturation magnetization of the amorphous matrix), the average anisotropy $\langle K_1 \rangle$ changes as [5]

$$\langle K_1 \rangle \propto K_1^4 D^6/(1 - T/T_{c,am})^{6\gamma} \tag{22}$$

where $T_{c,am}$ is the Curie temperature of the amorphous matrix, and $\gamma$ is the critical exponent. It is known that the domain wall width is inversely proportional to the square root of the anisotropy constant. Moreover, the disaccommodation intensity is proportional to $1/d$ (where $d$ is the domain wall width) [51]. Thus, the rapid increase of the disaccommodation intensity just below the Curie temperature of the amorphous matrix may be explained by the decrease of the domain wall thickness due to the increase of the average anisotropy $\langle K_1 \rangle$ (equation (23)).

However, it is important to emphasize that the increase of $\Delta(1/\chi)$ for the nanocrystalline alloys is also observed above the Curie temperature of the amorphous matrix (figure 5 and [52]). This effect and the behaviour of the magnetic susceptibility for the nanocrystalline samples (figure 2) near the Curie temperature of the amorphous matrix indicate that the fine $\alpha$-FeSi grains cannot be treated as non-interacting single-domain crystallites [53], because the distance between them is too small [54]. Thus, the exchange interaction propagates through paramagnetic layers of the amorphous matrix even at elevated temperatures, and should be taken into account in a full explanation of the magnetic properties of the nanocrystalline materials.

## 5. Conclusions

It is shown that the disaccommodation intensity and stabilization field decrease distinctly with annealing temperature and time. Furthermore, after cumulative annealing of the $Fe_{73.5}Cu_1Nb_3Si_{13.5}B_9$ alloy, only short-range order is found in the crystalline $\alpha$-FeSi phase. Moreover, the results obtained for this alloy indicate that the processes occurring in the amorphous matrix play the dominant role, as the main source of the magnetic after-effect in nanocrystalline alloys.

## Acknowledgments

The authors would like to thank Dr Jacek Olszewski of the Technical University of Częstochowa for helpful discussion concerning the analysis of the Mössbauer spectra, and Dr Grzegorz Haneczok from the Silesian University in Katowice for supplying the computer program used for the analysis of the isochronal disaccommodation curves.

This work was supported by the Committee for Scientific Research (Warsaw, Poland) (grant No 7T08A 007 10).

## References

[1] Yoshizawa Y and Yamauchi K 1990 *Mater. Trans. Japan Inst. Met.* **31** 307
[2] Herzer G 1990 *IEEE Trans. Magn.* **26** 1397
[3] Herzer G 1991 *Mater. Sci. Eng.* A **133** 1
[4] Herzer G 1992 *J. Magn. Magn. Mater.* **112** 258
[5] Herzer G 1989 *IEEE Trans. Magn.* **25** 3327
[6] Hofmann S B, Reininger T and Kronmüller H 1992 *Phys. Status Solidi* a **134** 247
[7] Lachowicz H K and Ślawska-Waniewska A 1994 *J. Magn. Magn. Mater.* **133** 238

[8] Müller M, Mattern N and Illgen L 1991 *Z. Metallk.* **82** 895
[9] Hiraga K and Kohmoto O 1991 *Mater. Trans. Japan Inst. Met.* **33** 868
[10] Zhou X Z and Morrish A H 1993 *J. Appl. Phys* **73** 6597
[11] Rixecker G, Schaaf P and Gonser U 1992 *J. Phys.: Condens. Matter* **4** 10 295
[12] Allia P and Vinai F 1982 *Phys. Rev.* B **26** 6141
[13] Kronmüller H 1983 *Phil. Mag.* B **48** 127
[14] Néel L 1952 *J. Physique Radium* **13** 249
[15] Kronmüller H 1968 *Nachwirkung in Ferromagnetika* (Berlin: Springer)
[16] Kröner E, Kronmüller H and Träube H 1965 *Moderne Probleme der Metall-physik* vol B2 (Berlin: Springer) p 122
[17] Néel L 1951 *J. Physique Radium* **12** 339
[18] Kronmüller H 1984 *J. Magn. Magn. Mater.* **41** 366
[19] Fish G E 1985 *IEEE Trans. Magn.* **21** 1996
[20] Kim K Y, Noh T H, Lee Y H, Kang J K and Kang T 1993 *J. Appl. Phys.* **73** 6595
[21] Grössinger R, Holzer D, Kussbach C, Sinnecker J P, Sato Turtelli R and Gahlgren M 1994 Nanostructured and non-crystalline materials *Proc. 4th Int. Workshop on Noncrystalline Solids (Madrid)* (Madrid: World Scientific)
[22] Polak C, Knobel M, Grössinger R and Sato Turtelli R 1994 *J. Magn. Magn. Mater.* **134** 1
[23] Gawior W and Woch M 1992 *J. Magn. Magn. Mater.* **111** 90
[24] Hesse J and Rübartsch A 1974 *J. Phys. E: Sci. Instrum.* **7** 526
[25] Greneche J M and Varret F 1982 *J. Phys. C: Solid State Phys.* **15** 985
[26] Pfannes H D and Fischer H 1977 *Appl. Phys.* **13** 317
[27] Jiang J, Aubertin F, Gonser U and Hilizinger H R 1991 *Z. Metallk.* **82** 698
[28] Kataoka N, Inoue A, Matsumoto T, Yoshizawa Y and Yamauchi K 1989 *Japan. J. Appl. Phys.* **28** L1820
[29] Pundt A, Hampel G and Hesse J 1992 *Z. Phys.* B **87** 65
[30] Gunnlangsson H P, Nilsen O V and Koch C B 1995 *Phys. Scr.* **52** 113
[31] Yang Huisheng, Tu Guochao, Xiong Xiaotao, Xu Zuxiong and Ma Ruzhang 1994 *J. Magn. Magn. Mater.* **138** 94
[32] Knobel M and Sato Turtelli R 1992 *J. Appl. Phys.* **71** 6008
[33] Zemčik T 1993 *Key Eng. Mater.* **81–3** 261
[34] Chien C L, Musser D, Gyorgy E M, Sherwood R C, Chen H S, Luborsky F E and Walter J L 1979 *Phys. Rev.* B **20** 283
[35] Mangin P and Marchal G 1978 *J. Appl. Phys.* **49** 1709
[36] Kopcewicz M, Drozowski W and Batkiewicz B 1985 *J. Magn. Magn. Mater.* **51** 218
[37] Preston R S, Hanna S S and Heberle J 1962 *Phys. Rev.* **128** 2207
[38] Litvinov V S, Karakishev S D and Ovchinnikov V V 1982 *Nuclear $\gamma$-Resonance Spectroscopy of Alloys* (Moscow: Metallurgia)
[39] Chen W Z, Li Z H and Zhang G X 1995 *J. Magn. Magn. Mater.* **146** 354
[40] Cserei A, Jiang J, Aubertin F and Gonser U 1994 *J. Mater. Sci.* **29** 1213
[41] Stearns M B 1963 *Phys. Rev.* **129** 1136
[42] Bogachev I N, Karakishev S D, Litvinov V S and Ovchinnikov V V 1974 *Phys. Status Solidi* a **24** 661
[43] Grimm H and Kronmüller H 1983 *Phys. Status Solidi* b **117** 663
[44] Reininger T, Moser N, Hofmann A and Kronmüller H 1988 *Phys. Status Solidi* a **110** 243
[45] Blythe H J and Gibbs M R J 1985 *J. Magn. Magn. Mater.* **53** 179
[46] Nowick A S and Berry B S 1972 *Anelastic Relaxation in Crystalline Solids* (New York: Academic)
[47] Bourrous M, Moser N and Kronmüller H 1989 *Phys. Status Solidi* a **112** 181
[48] Hisatake K, Miyazaki T, Takahashi M, Maeda K, Hattori T and Matsubara I 1986 *Phys. Status Solidi* a **93** 605
[49] Röss E 1966 *Z. Angew. Phys.* **21** 391
[50] Hisatake K and Ohta K 1973 *Japan. J. Appl. Phys.* **22** 1024
[51] Rasek J 1973 *Acta Phys. Pol.* A **44** 85
[52] Zbroszczyk J 1996 *Phys. Status Solidi* a **153** 507
[53] Pfeiffer H and Schüppel W 1994 *J. Magn. Magn. Mater.* **130** 92
[54] Hernando A and Kulik T 1994 *Phys. Rev.* B **49** 7064